Technical Improvements

2

Harald H. Quick

2.1 Introduction

Hybrid imaging with combined positron emission tomography/magnetic resonance (PET/MR) imaging is the most recent hybrid imaging modality (Drzezga et al. 2012; Quick et al. 2013). It combines excellent soft tissue contrast and high spatial image resolution of MR imaging with metabolic information provided by PET, as integrated PET/MR systems acquire PET and MR data simultaneously (Delso et al. 2011; Quick 2014; Grant et al. 2016). Beyond exact co-registration of PET and MR data, this can be applied for MR-based motion correction of PET data.

The integration of PET detectors within MR imaging systems has been a challenging task that has been solved by different vendors introducing three different PET/MR systems in the years 2010–2014 (Delso et al. 2011; Quick 2014; Grant et al. 2016; Zaidi et al. 2011). When compared to hybrid PET/computed tomography (CT), PET/MR has demonstrated comparable PET image quality and PET quantification in numerous clinical comparison studies (Drzezga et al. 2012; Quick et al. 2013; Wiesmüller et al. 2013). However, due to the missing CT component, attenuation correction in PET/MR has to be based on MR images and subsequent image segmentation. This turned out to be challenging and a wealth of methodological developments have been described in the recent literature.

Ultimately, the aim of all current technical and methodological developments in PET/MR is to further improve workflow, image quality, PET quantification, and to broaden the application spectrum of PET/MR in research and clinical applications. This chapter on technical developments highlights current developments in PET/MR attenuation correction and motion correction, introduces new hardware developments, and discusses current research efforts on artifact correction and dose reduction in PET/MR hybrid imaging.

2.2 Attenuation Correction in PET/MR

PET is a quantitative imaging technique that facilitates the determination of the amount of radioactive tracer accumulation in a tumour, lesion or organ within the human body. In this context, attenuation correction (AC) describes a physical method to account for the self-absorption of the emitted annihilation photons in tissue and

H.H. Quick, Ph.D.
Erwin L. Hahn Institute for MR Imaging, University of Duisburg-Essen, Essen, Germany

High Field and Hybrid MR Imaging, University Hospital Essen, Essen, Germany
e-mail: harald.quick@uni-due.de

L. Umutlu, K. Herrmann (eds.), *PET/MR Imaging: Current and Emerging Applications*,
https://doi.org/10.1007/978-3-319-69641-6_2

in hardware components. Attenuation correction, thus, is a pre-requisite for accurate quantification of the PET data (Kinahan et al. 1998). More specifically, the photons that originate from a positron annihilation within the body are attenuated by the surrounding tissues and by ancillary hardware components such as the patient table before they reach the PET detectors.

In combined PET/CT systems, the attenuation properties of tissue can be derived from the complementary CT images after a fast and straightforward conversion of the photon energy levels of CT-derived Hounsfield units (HU) to linear attenuation coefficients (LAC) for PET (Kinahan et al. 1998; Carney et al. 2006). In PET/MR, however, attenuation correction is methodologically challenging (Wagenknecht et al. 2013) as MR imaging measures magnetization densities and relaxation times of hydrogen nuclei in tissue. The MR signal, thus, depends on the amount of protons and their local chemical environment in tissues. As there is no direct physical dependency of proton density and proton spin relaxation times with local electron density, which causes the photon attenuation, it is not possible to derive PET attenuation properties of tissues directly from MR imaging measurements (Wagenknecht et al. 2013). To address this issue, different concepts for attenuation correction in PET/MR have been developed (Wagenknecht et al. 2013). The most widely used method for MR-based attenuation correction relies on the segmentation of MR images into different tissue classes, based on their image-based grey scales. Following segmentation, the individual tissue compartments (e.g., background air, fat, soft tissue, lung tissue) are then assigned a predefined LAC for the corresponding tissue (Martinez-Moller et al. 2009; Schulz et al. 2011). To this day, dedicated fast MR imaging sequences, such as Dixon VIBE (Martinez-Moller et al. 2009) or a fast 3D T1-weighted gradient-echo MR sequence, are applied to obtain images of tissue distribution and subsequent segmentation (Beyer et al. 2016). This general method of tissue segmentation from MR images is widely used in all currently available PET/MR systems (Beyer et al. 2016) (Fig. 2.1).

Although the MR-based segmentation techniques for AC in general provide reproducible and straightforward results in most clinical applications, multiple initial studies directly comparing PET quantification in PET/MR with PET/CT have indicated a small but systematic underestimation of PET quantification in PET/MR studies using these MR-based AC methods (Drzezga et al. 2012; Quick et al. 2013; Wiesmüller et al. 2013; Boellaard and Quick 2015). The observed underestimation of PET quantification in PET/MR can be attributed to three methodological challenges of MR-based AC: First, MR-based AC lacks information about the attenuating properties of bone. Second, MR-imaging based AC often shows signal truncations along the patient arms, that are then not considered in MR-based AC. Third, the use of ancillary hardware components, such as RF coils in the field-of-view (FOV) of the PET-detector during simultaneous PET and MR data acquisition cause additional attenuation of photons (Boellaard and Quick 2015).

2.3 Attenuation Correction of Bone

Cortical bone is not considered in the standard MR-based AC approaches. Bone here is classified as soft tissue, consequently, the exact magnitude of PET signal attenuation of bone might be systematically underestimated (Samarin et al. 2012; Akbarzadeh et al. 2013). Samarin et al. (Samarin et al. 2012) evaluated and quantified the amount of underestimation when bone is assigned the linear attenuation coefficient of soft tissue. It was shown, that for most soft-tissue lesions in whole-body examinations, PET quantification would be biased by a few %-points only. In brain PET/MR and when imaging individual bone lesions, however, the classification of bone as soft-tissue causes a significant and regionally variable bias of 20–30% (Samarin et al. 2012). As potential solutions for AC of bone, the use of MR sequences with ultrashort echo times (UTE) (Keereman et al. 2010; Johansson et al. 2011; Navalpakkam et al. 2013; Berker et al. 2012; Grodzki et al. 2012) or zero echo time (ZTE) have been

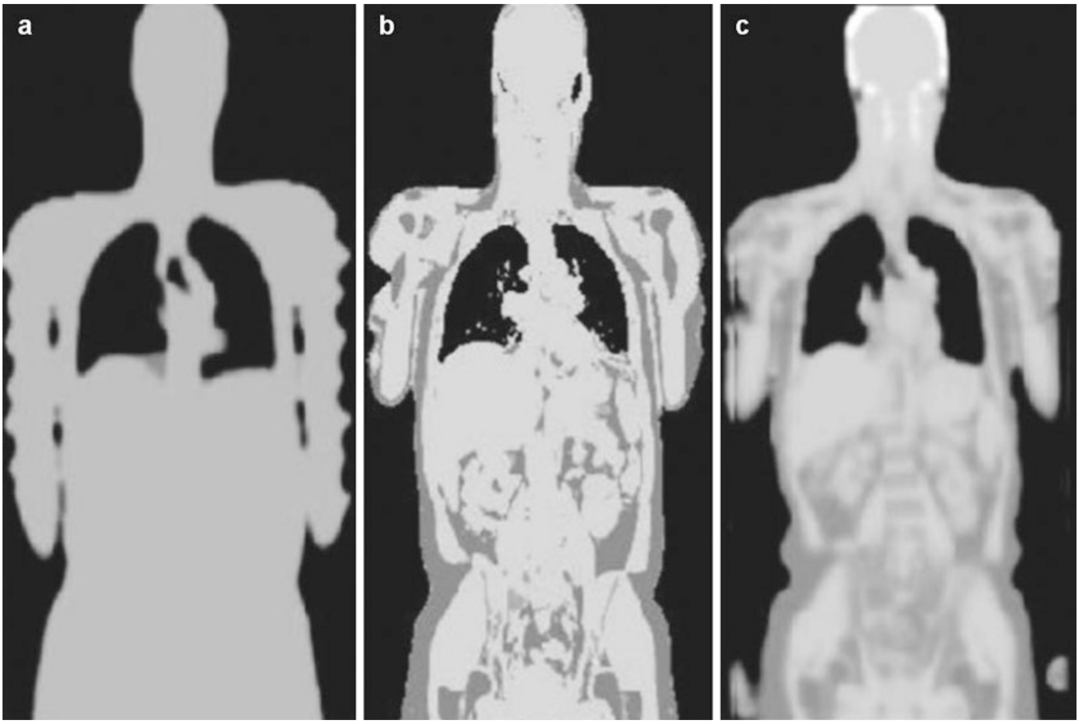

Fig. 2.1 Whole-body MR-based attenuation correction maps in coronal orientation. The AC maps were acquired by scanning one volunteer on all three current PET/MR systems, the Philips Ingenuity TF PET/MR (**a**), the Siemens Biograph mMR (**b**), and the GE Signa PET/MR (**c**). Note that MR-based AC in (**a**) provides three attenuation classes (background, soft tissue and lung), while MR-based AC in (**b** and **c**) provides four classes (background, fat, soft tissue, lung). At the time of this study (2014), system (**c**) additionally provided bone in the head station based on ultrashort echo time sequences. All three AC maps are limited by field-of-view truncations along the arms. Another general limitation in AC is the substitution of major bones by the attenuation coefficients of soft tissue. The figure reflects the state of MR-based AC in the year of measurement, i.e. 2014 (Beyer et al. 2016). To date (2017) further improvements such as bone detection and MR-based truncation correction have been implemented into new product software versions of the PET/MRI systems. (Modified from Beyer et al. 2016)

proposed (Wiesinger et al. 2016; Delso et al. 2015). While studies have shown that UTE-based AC provide accurate PET quantification results when imaging the brain (Johansson et al. 2011; Navalpakkam et al. 2013), their use in body imaging applications is limited (Aasheim 2015). Here, the fact that UTE and ZTE sequences tend to increase image artifacts in large FOV applications such as in body imaging (Navalpakkam et al. 2013) is a practical limitation.

A fast and practical solution for bone AC in whole-body PET/MR has recently been suggested and evaluated (Paulus et al. 2015). This method applies a CT-based 3-dimensional bone-model of the major bones (skull, spine, pelvic bones, upper femora) to the actual MR-based AC data of the patient under examination and, thus, adds another compartment for the AC of bone in whole-body PET/MR exams (Fig. 2.2) (Paulus et al. 2015). This method has recently been validated in whole-body and brain PET/MR exams with promising results towards improved MR-based AC (Paulus et al. 2015; Koesters et al. 2016; Rausch et al. 2017; Oehmigen et al. 2017).

2.4 Truncation Correction

Another limitation of MR-based AC is the fact that the transaxial FOV in MR imaging is limited to about 50 cm in diameter. Beyond these dimensions, MR images show geometric distortions and

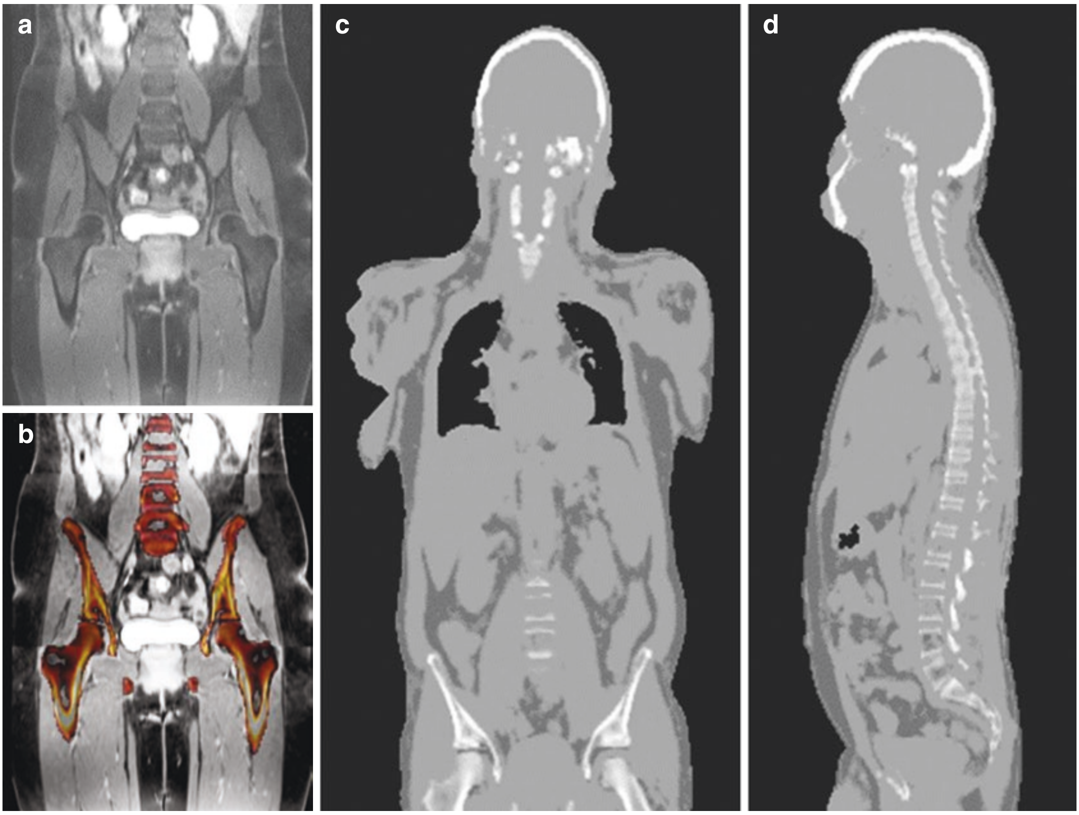

Fig. 2.2 Example for model-based addition of major bones to patient-individual MR data as shown for the pelvic region (**a**, **b**). The bone model consists of a set of MR image and bone mask pairs that are registered to subject's Dixon-sequence images for each major bone individually. Panels (**c** and **d**) show the result of adding bone as additional attenuation class to a whole-body MR-based attenuation map in coronal and sagittal orientation, respectively. (Modified from Paulus et al. 2015)

significant signal voids (Keller et al. 2013; Brendle et al. 2015a). This frequently results in truncation artifacts along the patient arms in MR-based AC, as has been shown for all three currently available PET/MR system designs (Beyer et al. 2016). Therefore, the patient body is not completely and correctly assessed in its overall dimensions and current shape. Thus, the human tissue AC based on truncated MR images does not consider the exact amount and position of tissues that contribute to PET signal attenuation, resulting in inaccurate values for PET quantification (Delso et al. 2010a; Schramm et al. 2013). Accurate PET quantification in PET/MR, thus, requires appropriate methods for truncation correction as part of the attenuation correction strategy.

An appropriate method for truncation correction that is used on all three currently available PET/MR systems is the so-called MLAA (maximum likelihood estimation of attenuation and activity) algorithm (Nuyts et al. 1999, 2013). This PET-based technique derives the outer patient contours from non-AC PET data. This information is then used to complement missing attenuation information from MR imaging data that is truncated due to the limited transaxial FOV of MR imaging (Nuyts et al. 2013). However, MLAA-based contour detection is mostly limited to radiotracers that show a considerable unspecific accumulation in the human body and blood pool, thus enabling the detection of the outer patient contour from PET signals.

Fig. 2.3 Example for a MR-based attenuation map showing the typical lateral signal truncations along the subjects arms in coronal and transaxial orientation (**a**). Truncations result from the limited field-of-view in MR imaging. Image (**b**) was acquired by applying an optimized readout gradient field provided with the HUGE-method (Blumhagen et al. 2012, 2014). This results in a field-of-view extension and enables truncation correction of the MR-based attenuation correction maps (**b**). Truncation correction of the arms in (**c**) was achieved by applying the widely established MLAA method that derives truncated regions from PET data. The difference map in (**d**) visualizes the quantification bias (in %) between images (**a**) and (**b**), i.e. the quantitative gain by applying HUGE truncation correction. Note that truncation correction applied along the arms has also quantitative impact on the entire body volume (red and blue areas in (**d**)). (Modified from Lindemann et al. 2017)

Another method for truncation correction based on MR data was developed by Blumhagen et al. (Blumhagen et al. 2012). The method is referred to as HUGE ((B_0 homogenization using gradient enhancement) and enlarges the field-of-view in MR imaging beyond the conventional 50 cm diameter (Blumhagen et al. 2012). Foundation of the HUGE method is the measurement of the static magnetic field (B0) and gradient field distributions in the specific PET/MR system. Then, an ideal, non-distorted gradient field is calculated that is applied during MR-based AC in the lateral regions of the MR imaging FOV (Blumhagen et al. 2012). Thus, the lateral MR-based field-of-view can be extended to 60 cm in left-right direction to fully cover the patient's arms. The HUGE method has been successfully evaluated for truncation correction in whole-body PET/MR examinations in the past (Blumhagen et al. 2014). Further technical refinements of the prototype sequence and the combination of HUGE with a moving table acquisition have now resulted in the product version of HUGE that provides seamless MR data for truncation correction in PET/MR (Lindemann et al. 2017) (Fig. 2.3).

2.5 Motion Correction

The independent and simultaneous PET and MR data acquisition in integrated PET/MR systems inherently offers the potential for motion correction and co-registration of PET and MR data (Quick 2014). This can be considered a potential advantage over PET/CT, which is currently being further explored (Tsoumpas et al. 2010; Tsoumpas et al. 2011; Wuerslin et al. 2013; Grimm et al. 2015; Baumgartner et al. 2014; Catana 2015; Manber et al. 2015; Fürst et al. 2015; Fayad et al. 2015; Gratz et al. 2017). In PET/CT the CT data is static and is acquired only once at the beginning of a typical hybrid examination. Since CT data acquisition is very fast (seconds), CT images provides a snapshot of the body anatomy and state of motion at the time of data acquisition while whole-body PET data is acquired stepwise over several minutes. In

PET/MR, the MR data is acquired simultaneous to PET data, which usually takes several minutes, both for PET and MR data. This leads to less deviation and less gross motion between both imaging modalities when compared to PET/CT hybrid imaging (Brendle et al. 2013). Moreover, real-time MR imaging and 4D MR data of breathing motion can be used to retrospectively perform motion correction of PET data, providing improved fusion of PET and MR data sets (Tsoumpas et al. 2010; 2011; Wuerslin et al. 2013; Grimm et al. 2015; Baumgartner et al. 2014; Catana 2015; Manber et al. 2015; Fürst et al. 2015; Fayad et al. 2015; Gratz et al. 2017). Motion correction strategies in PET/MR, thus, potentially lead to improved lesion visibility in the upper abdomen and liver (Fig. 2.4). Additionally, motion correction may also result in better quantification of activity in lesions and tumours as well as in cardiovascular PET/MR studies since all moving structures are depicted with sharper contours and less smeared over a larger volume, which otherwise leads to reduced standardized uptake values (SUV) of regions subject to motion (Grimm et al. 2015) (Fig. 2.4). In a recent cardiac PET/MR feasibility study, motion correction strategies have been applied to breathing and cardiac motion to assess atherosclerotic plaques in the coronary arteries (Robson et al. 2017).

2.6 Attenuation Correction of Hardware Components

The previous sections have discussed techniques, limitations, and recent solutions for MR-based AC of the patient body. An additional source of attenuation of the annihilation photons in PET/MR is the use of ancillary hardware components, such as the patient table and radiofrequency (RF) receiver coils that are placed around the patient body for MR signal detection. These hardware components also attenuate photons before they reach the PET detector and, therefore, may cause a bias of the PET quantification, as demonstrated in earlier studies (Delso et al. 2010b; Tellmann et al. 2011). The general concept for AC of hardware components in PET/MR is to generate CT-based attenuation maps of each hardware component that has to be corrected (Quick et al. 2013; Quick 2014), as it is the current standard method on all three current PET/MR systems. Therefore, three-dimensional (3D) CT-based

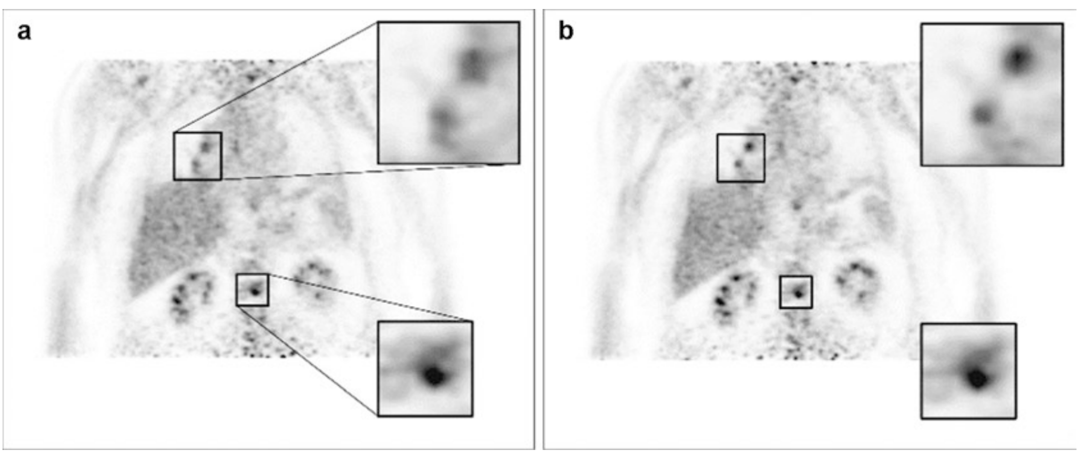

Fig. 2.4 Application of motion correction in a patient with two lesions in the lung and one lesion in the spine. A coronal PET image from a PET/MR study is shown. Image (**a**) was acquired using the standard free-breathing PET protocol with an acquisition time of several minutes. Image (**b**) was acquired by applying respiratory motion correction. For motion correction the MR data was used to derive 3-dimensional motion fields over time that were then used for non-rigid registration of the PET data to one static, motion corrected 3D image. The motion corrected data in (**b**) provides sharper visualization and higher contrast of the two lesions in the lung, while the non-moving lesion in the spine shows identical image features (Modified from Gratz et al. 2017)

attenuation templates for rigid and stationary RF coils such as the head/neck RF coil are added to the overall patient attenuation map prior to the PET data reconstruction (Quick 2014). By automatically linking the current patient table position during a patient examination to the known position of the individual RF coil on the system's patient table, CT-template-based AC can be performed during the PET data reconstruction process (Delso et al. 2010b). This AC method provides fast and accurate results for most of the RF coils that are delivered with the current PET/MR systems. However, the 3D attenuation templates used during reconstruction can be misaligned with the actual RF coil position or not represent the actual attenuation of the RF coils used (Paulus et al. 2012). This is an inherent limitation for flexible (non-rigid) RF surface coils, which are frequently used in whole-body imaging applications to provide excellent MRI signal from the anterior body parts. Flexible RF coils are currently not routinely considered in CT-template-based AC since their position and/or geometry during a PET/MR examination is not known and may differ from a pre-acquired 3D AC template (Paulus et al. 2012). It has been shown in previous studies, that the flexible standard multi-channel RF surface body coils attenuate the PET signal by only few %-points (Paulus et al. 2012, 2013; Wollenweber et al. 2014; Paulus and Quick 2016). Thus, the average attenuation due to flexible RF coils in routine applications of PET/MR seems negligible. However, PET quantification may be locally biased by up to 10–20% due to increased attenuation of PET signal in the immediate vicinity of single hardware components of the RF coils (Paulus et al. 2012, 2013; Paulus and Quick 2016). As an improvement to also consider flexible RF coils in AC, it has been suggested to detect the actual position of flexible RF coils in MR images by using MR visible markers (Kartmann et al. 2013; Eldib et al. 2014) or by using residual MR signal from the RF coil housing when applying UTE sequences (Paulus et al. 2012; Eldib et al. 2015). This spatial information could then be used to align a pre-defined 3D AC template of the respective RF coil with its actual position during a PET/MR examination as derived from MR images. The general concept for CT-based AC of hardware components in PET/MR is implemented in all currently available PET/MR systems for the range of rigid RF coils that are delivered with each PET/MR system (Quick 2014; Paulus and Quick 2016).

2.7 New Hardware Developments

The current PET/MR systems are all equipped with numerous RF coils to cover the patient from head to toe in whole-body imaging applications (Quick 2014; Beyer et al. 2016). Coverage of the entire patient body with RF surface coils is a general precondition for high quality MR imaging. In combined PET/MR, the RF coils are located in the FOV of the PET detector during simultaneous PET and MRI data acquisition. Thus, an additional design requirement for RF coil in PET/MR is, that the RF coils need to be as PET transparent as possible in order to reduce unwanted PET signal attenuation. Nevertheless, although designed PET transparent, all RF coils are subject to attenuation correction to provide accurate PET quantification as has been described in the previous section. A recent overview article by Paulus and Quick (2016) provides a summary of numerous RF coil developments for PET/MR applications and their individual impact on PET quantification (Paulus and Quick 2016).

To expand the portfolio of clinical applications of PET/MR and to improve dedicated examinations, new and specific RF coils were designed over the recent years for combined use in PET/MR. For example, new multi-channel RF head coils have been designed to improve neuro imaging and to increase the perfomance of simultaneous functional MR imaging (fMRI) with PET imaging (Sander et al. 2015). Three recent studies have described the design and implementation of bilateral breast RF coils for PET/MR breast imaging (Aklan et al. 2013; Dregely et al. 2015; Oehmigen et al. 2016). The integration of such breast RF coils requires a PET-transparent design and consideration of the ancillary RF coil

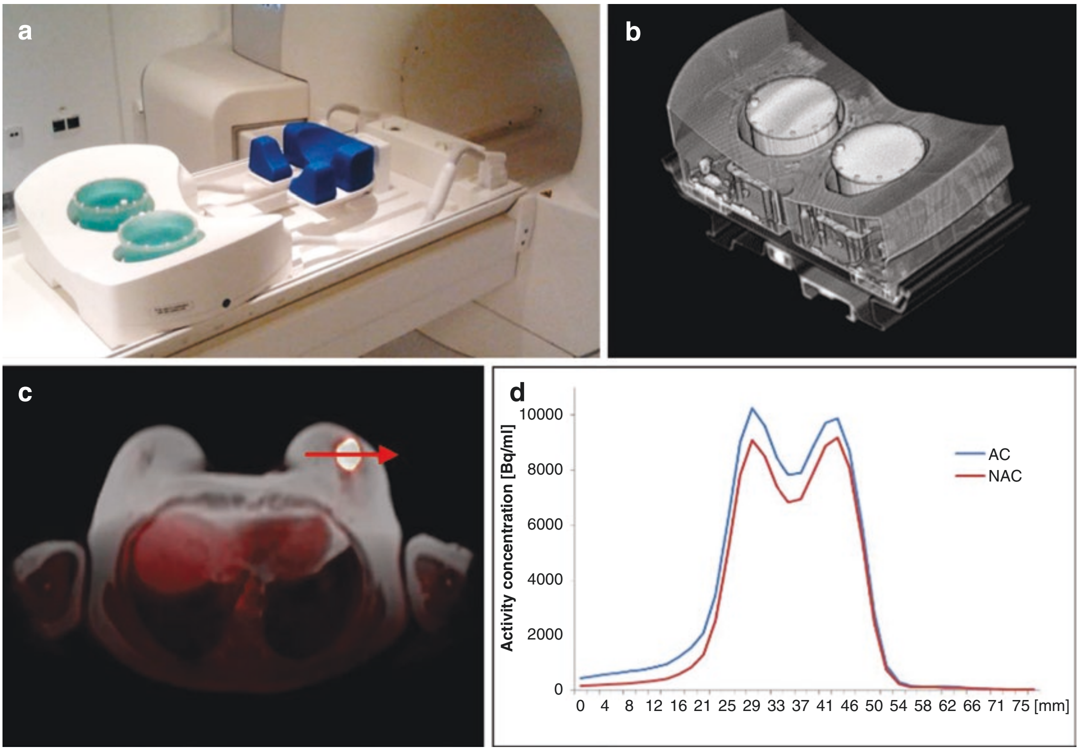

Fig. 2.5 Broadening the application spectrum of PET/MR by integration of a breast radiofrequency (RF) coil. 16-channel breast RF coil that was designed PET transparent for use in PET/MR systems (Rapid Biomedical, Germany) (**a**). (**b**) 3-Dimensional CT-based attenuation template for attenuation correction of the RF coil housing. (**c**) Example case of patient with breast carcinoma imaged on PET/MR with the RF breast coil. (**d**) Quantitative evaluation of activity concentration in the breast tumour along the red arrow (in **c**). The blue line plot shows the activity in the tumour after attenuation correction of the RF breast coil. The red line plot shows lower activity values because the RF breast coil here was not included in attenuation correction. (Modified from Oehmigen et al. 2016)

hardware in the attenuation correction (Aklan et al. 2013; Dregely et al. 2015, 2016). Figure 2.5 provides an example of a 16-channel breast RF coil that was implemented into an integrated PET/MR system with hardware attenuation correction (Oehmigen et al. 2016).

Two recent studies describe the development of equipment for radiation therapy (RT) planning for use in PET/MR. The overall aim of this endeavour is to integrate PET/MR hybrid imaging into the concept of RT planning, which would further broaden the application spectrum of PET/MR (Paulus et al. 2014, 2016). The developments encompass PET transparent hardware components such as a table platform with indexing system and RF coil holders for head/neck imaging as well as for body imaging (Paulus et al. 2014, 2016). All components have been evaluated for use in PET/MR. A systematic µmap generator ensures accurate attenuation correction of all RT equipment in the FOV of the PET detector (Paulus et al. 2014). All these recent RF coil and hardware component developments have laid the groundwork for new clinical applications of PET/MR and further developments of dedicated RF coils are ongoing. The additional efforts in hardware component AC at the same time ensure accurate PET quantification for these exciting new applications (Paulus and Quick 2016).

2.8 Artifact Correction

The implementation of new imaging modalities and / or technical systems goes hand in hand with new types of artifacts. The complexity of integrated PET/MR hybrid imaging bears the potential for an exaggeration of new artifacts, when compared to two independent systems. Beyond the potential affection of the visual impression of either PET or MR data, artifacts in PET/MR may also have a significant effect on quantification of PET data. Artifacts in integrated PET/MR may result from the technical crosstalk between the PET and the MR components (Delso et al. 2011; Quick 2014), e.g. when both imaging centers may not be co-aligned correctly (Brendle et al. 2013). Differences in the data acquisition speed between PET and MR might lead to local misalignments and motion artifacts due to patient and organ motion (Brendle et al. 2013). In MR-based AC all deviations from the real physical photon attenuation will ultimately lead to inaccurate values in PET quantification following AC (Keereman et al. 2011; Ladefoged et al. 2014; Brendle et al. 2015). Furthermore, the administration of contrast agents before the application of MR-based AC may lead to errors in MR-based tissue segmentation due to changes in tissue contrast (Ruhlmann et al. 2016). Per definition, the signal truncations as discussed above also represent MR-based artifacts that have an influence on PET quantification (Delso et al. 2010a; Blumhagen et al. 2012, 2014). A frequent source for MR-based artifacts are dental and metal implants that are found in a large and increasing group of patients (Gunzinger et al. 2014; Ladefoged et al. 2015; Schramm et al. 2014). Apart from the safety aspects of metal implants that have to be clarified for any MR examination, all metal implants might cause signal voids or local distortions in MR images and in MR-based AC, that exceed the physical implant volume. During image segmentation, such signal voids might then be assigned with the low linear attenuation coefficients of air (Gunzinger et al. 2014; Ladefoged et al. 2015; Schramm et al. 2014).

While initial publications dealt with the description of artifacts and evaluation of their impact on PET/MR, more recent studies now report about developments to correct for artifacts. A relatively simple approach to improve the MR-based μmap, is to use inpainting to fill signal voids arising from metal artifacts (Ladefoged et al. 2013). Thus, signal voids simulating regions with the low LAC of air are removed and the higher value LAC of the surrounding tissue is assigned (Ladefoged et al. 2013). Beyond the visual improvement of data, this may improve PET quantification as well. However, when larger metal and ceramic implants such as knee or hip joints are involved, PET quantification following μmap inpainting will still be biased due to the fact, that the real high LAC of these metallic implants is not accurately considered. Fuin et al. have suggested a method to complete signal voids in the MR-based attenuation correction data caused by implants by deriving the shape and AC values of metal implants from PET emission data (Fuin et al. 2017). In the context of metal artifact reduction in PET/MR, it has been shown that time-of-flight (TOF) PET detection with fast PET detectors allows for a significant visual reduction of artifacts in the μmap (Davison et al. 2015; Ter Voert et al. 2017), albeit PET quantification may still be biased. For the near future, it is expected that also the current breed of new artifact reducing MR imaging sequences (e.g. MAVRIC, VAT, WARP, etc.) (Sutter et al. 2012; Talbot and Weinberg 2016; Dillenseger et al. 2016; Jungmann et al. 2017) will find their implementation in dedicated PET/MR imaging protocols. In MR-only applications, such sequences have facilitated a significant reduction of the volume of distortions and signal voids around metallic implants (Sutter et al. 2012; Talbot and Weinberg 2016; Dillenseger et al. 2016; Jungmann et al. 2017). In the PET/MR regime, this could be used to further improve μmaps, and consequently, to improve PET quantification in PET/MR of patients with implants.

2.9 Dose Reduction

Integrated PET/MR hybrid imaging in selected clinical applications inherently reduces the overall patient radiation dose when compared with PET/CT by replacing ionizing CT imaging by non-ionizing MR imaging (Boellaard et al.

2010). Depending on the clinical indication, replacing CT by MR imaging in the context of PET hybrid imaging theoretically may save half of the overall radiation dose or an even higher fraction when compared with high-resolution diagnostic CT imaging (Boellaard et al. 2010). Further potential for radiotracer dose reduction in integrated PET/MR resides in the possibility of decreasing the applied activity deriving from the administered PET radiotracer. PET image quality in general is influenced by two key factors, acquisition time and injected activity, as both affect count statistics, image signal, and image noise. In PET/MR imaging, radiotracer dose reduction by injecting less tracer activity may be achieved by turning the comparatively prolonged data acquisition times into an advantage. In conventional PET/CT hybrid imaging, the PET data acquisition times typically amount to 2–3 min per bed position (Boellaard et al. 2010). In integrated PET/MR hybrid imaging, the MR examination time may be longer depending on the study protocol and clinical application field, respectively.

The higher sensitivity and larger volume coverage of new PET detectors in PET/MR systems compared to PET/CT (Delso et al. 2011) provides a third precondition for the potential to reduce the applied activity while maintaining high SNR and excellent PET image quality (Queiroz et al. 2015).

These potential advantages of PET/MR towards reducing the overall radiation dose compared to PET/CT is currently explored in selected studies. Based on the findings in controlled phantom studies (Oehmigen et al. 2014), or by simulating reduced amounts of applied activity by shortening the acquired PET list-mode data (Hartung-Knemeyer et al. 2013; Gatidis et al. 2016c), initial studies indicate that the reduction of radiotracer does not hamper diagnostic image quality in PET/MR examinations (Hartung-Knemeyer et al. 2013; Seith et al. 2017). These efforts can be considered particularly important in clinical settings for pediatric imaging or repetitive scans for therapy monitoring or surveillance (Gatidis et al. 2016a, b).

Conclusion

Today, many of the technical and methodological challenges of PET/MR imaging that were considered roadblocks to clinical PET/MRI during the early phase of implementation have been overcome. Numerous innovative solutions for attenuation correction, truncation correction, and motion correction have been suggested and scientifically evaluated during the past years. Of these, some of the most accurate and practical developments have found their way from research applications into the most recent product software applications of all PET/MR systems. Together with further hardware developments, this emerging hybrid imaging method is constantly improved and the clinical application spectrum of PET/MR is further increased.

References

Aasheim LB, Karlberg A, Goa PE, et al. PET/MR brain imaging: evaluation of clinical UTE-based attenuation correction. Eur J Nucl Med Mol Imaging. 2015;42(2015):1439–46.

Akbarzadeh A, Ay MR, Ahmadian A, Alam NR, Zaidi H. MRI-guided attenuation correction in whole-body PET/MR: assessment of the effect of bone attenuation. Ann Nucl Med. 2013;27:152–62.

Aklan B, Paulus DH, Wenkel E, Braun H, Navalpakkam BK, Ziegler S, Geppert C, Sigmund EE, Melsaether A, Quick HH. Toward simultaneous PET/MR breast imaging: systematic evaluation and integration of a radiofrequency breast coil. Med Phys. 2013;40(2):024301.

Baumgartner CF, Kolbitsch C, Balfour DR, Marsden PK, McClelland JR, Rueckert D, King AP. High-resolution dynamic MR imaging of the thorax for respiratory motion correction of PET using groupwise manifold alignment. Med Image Anal. 2014;18:939–52.

Berker Y, Franke J, Salomon A, Palmowski M, Donker HC, Temur Y, Mottaghy FM, Kuhl C, Izquierdo-Garcia D, Fayad ZA, Kiessling F, Schulz V. MRI-based attenuation correction for hybrid PET/MRI systems: a 4-class tissue segmentation technique using a combined ultra-short-echo-time/Dixon MRI sequence. J Nucl Med. 2012;53:796–804.

Beyer T, Lassen ML, Boellaard R, Delso G, Yaqub M, Sattler B, Quick HH. Investigating the state-of-the-art in whole-body MR-based attenuation correction: an intra-individual, inter-system, inventory study on three clinical PET/MR systems. MAGMA. 2016;29:75–87.

Blumhagen JO, Braun H, Ladebeck R, Fenchel M, Faul D, Scheffler K, Quick HH. Field of view extension and truncation correction for MR-based human attenuation correction in simultaneous MR/PET imaging. Med Phys. 2014;41:022303.

Blumhagen JO, Ladebeck R, Fenchel M, Scheffler K. MR-based field-of-view extension in MR/PET: B(0) homogenization using gradient enhancement (HUGE). Magn Reson Med. 2012;70:1047–57.

Boellaard R, O'Doherty MJ, Weber WA, et al. FDG PET and PET/CT: EANM procedure guidelines for tumor PET imaging—version 1.0. Eur J Nucl Med Mol Imaging. 2010;37:181–200.

Boellaard R, Quick HH. Current image acquisition options in PET/MR. Semin Nucl Med. 2015;45:192–200. Review

Brendle C, Schmidt H, Oergel A, Bezrukov I, Mueller M, Schraml C, Pfannenberg C, la Fougère C, Nikolaou K, Schwenzer N. Segmentation-based attenuation correction in positron emission tomography/magnetic resonance: erroneous tissue identification and its impact on positron emission tomography interpretation. Investig Radiol. 2015a;50(5):339–46.

Brendle C, Schmidt H, Oergel A, Bezrukov I, Mueller M, Schraml C, Pfannenberg C, la Fougère C, Nikolaou K, Schwenzer N. Segmentation-based attenuation correction in positron emission tomography/magnetic resonance: erroneous tissue identification and its impact on positron emission tomography interpretation. Investig Radiol. 2015b;50(5):339–46.

Brendle CB, Schmidt H, Fleischer S, Braeuning UH, Pfannenberg CA, Schwenzer NF. Simultaneously acquired MR/PET images compared with sequential MR/PET and PET/CT: alignment quality. Radiology. 2013;268(1):190–9.

Carney JP, Townsend DW, Rappoport V, Bendriem B. Method for transforming CT images for attenuation correction in PET/CT imaging. Med Phys. 2006;33:976–83.

Catana C. Motion correction options in PET/MRI. Semin Nucl Med. 2015;45:212–23. Review

Davison H, ter Voert EE, de Galiza Barbosa F, Veit-Haibach P, Delso G. Incorporation of time-of-flight information reduces metal artifacts in simultaneous positron emission tomography/magnetic resonance imaging: a simulation study. Investig Radiol. 2015;50(7):423–9.

Delso G, Furst S, Jakoby B, Ladebeck R, Ganter C, Nekolla SG, et al. Performance measurements of the Siemens mMR integrated whole-body PET/MR scanner. J Nucl Med. 2011;52:1914–22.

Delso G, Martinez-Möller A, Bundschuh RA, Ladebeck R, Candidus Y, Faul D, Ziegler SI. Evaluation of the attenuation properties of MR equipment for its use in a whole-body PET/MR scanner. Phys Med Biol. 2010b;55:4361–74.

Delso G, Martinez-Möller A, Bundschuh RA, Nekolla SG, Ziegler SI. The effect of limited MR field of view in MR/PET attenuation correction. Med Phys. 2010a;37:2804–12.

Delso G, Wiesinger F, Sacolick LI, Kaushik SS, Shanbhag DD, Hüllner M, Veit-Haibach P. Clinical evaluation of zero-echo-time MR imaging for the segmentation of the skull. J Nucl Med. 2015;56(3):417–22.

Dillenseger JP, Molière S, Choquet P, Goetz C, Ehlinger M, Bierry G. An illustrative review to understand and manage metal-induced artifacts in musculoskeletal MRI: a primer and updates. Skelet Radiol. 2016;45(5):677–88. https://doi.org/10.1007/s00256-016-2338-2. Epub 2016 Feb 2. Review.

Dregely I, Lanz T, Metz S, Mueller MF, Kuschan M, Nimbalkar M, Bundschuh RA, Ziegler SI, Haase A, Nekolla SG, Schwaiger M. A 16-channel MR coil for simultaneous PET/MR imaging in breast cancer. Eur Radiol. 2015;25(4):1154–61.

Drzezga A, Souvatzoglou M, Eiber M, Beer AJ, Fürst S, Martinez-Möller A, Nekolla SG, Ziegler S, Ganter C, Rummeny EJ, Schwaiger M. First clinical experience with integrated whole-body PET/MR: comparison to PET/CT in patients with oncologic diagnoses. J Nucl Med. 2012;53:845–55.

Eldib M, Bini J, Calcagno C, Robson PM, Mani V, Fayad ZA. Attenuation correction for flexible magnetic resonance coils in combined magnetic resonance/positron emission tomography imaging. Investig Radiol. 2014;49:63–9.

Eldib M, Bini J, Robson PM, Calcagno C, Faul DD, Tsoumpas C, Fayad ZA. Markerless attenuation correction for carotid MRI surface receiver coils in combined PET/MR imaging. Phys Med Biol. 2015;60:4705–17.

Fayad H, Schmidt H, Wuerslin C, Visvikis D. Reconstruction-incorporated respiratory motion correction in clinical simultaneous PET/MR imaging for oncology applications. J Nucl Med. 2015;56:884–9.

Fuin N, Pedemonte S, Catalano OA, Izquierdo-Garcia D, Soricelli A, Salvatore M, Heberlein K, Hooker JM, Van Leemput K, Catana C. PET/MRI in the presence of metal implants: completion of the attenuation map from PET emission data. J Nucl Med. 2017;58(5):840–5.

Fürst S, Grimm R, Hong I, Souvatzoglou M, Casey ME, Schwaiger M, Nekolla SG, Ziegler SI. Motion correction strategies for integrated PET/MR. J Nucl Med. 2015;56:261–9.

Gatidis S, Schmidt H, Gücke B, Bezrukov I, Seitz G, Ebinger M, Reimold M, Pfannenberg CA, Nikolaou K, Schwenzer NF, Schäfer JF. Comprehensive oncologic imaging in infants and preschool children with substantially reduced radiation exposure using combined simultaneous ^{18}F-fluorodeoxyglucose positron emission tomography/magnetic resonance imaging: a direct comparison to ^{18}F-fluorodeoxyglucose positron emission tomography/computed tomography. Investig Radiol. 2016b;51(1):7–14.

Gatidis S, Schmidt H, la Fougère C, Nikolaou K, Schwenzer NF, Schäfer JF. Defining optimal tracer activities in pediatric oncologic whole-body ^{18}F-FDG-PET/MRI. Eur J Nucl Med Mol Imaging. 2016a;43(13):2283–9.

Gatidis S, Würslin C, Seith F, Schäfer JF, la Fougère C, Nikolaou K, Schwenzer NF, Schmidt H. Towards tracer dose reduction in PET studies: Simulation of dose reduction by retrospective randomized undersampling of list-mode data. Hell J Nucl Med. 2016c;19(1):15–8. https://doi.org/10.1967/s002449910333. Epub 2016 Mar 1

Grant AM, Deller TW, Khalighi MM, Maramraju SH, Delso G, Levin CS. NEMA NU 2-2012 performance studies for the SiPM-based ToF-PET component of the GE SIGNA PET/MR system. Med Phys. 2016;43:2334.

Gratz M, Ruhlmann V, Umutlu L, Fenchel M, Quick HH. Impact of MR-based motion correction on clinical PET/MR data of patients with thoracic pathologies. In Proc. ISMRM 2017, Apr 21–27; Honolulu, HI, USA. 2017 p. 3899.

Grimm R, Fürst S, Souvatzoglou M, Forman C, Hutter J, Dregely I, Ziegler SI, Kiefer B, Hornegger J, Block KT, Nekolla SG. Self-gated MRI motion modeling for respiratory motion compensation in integrated PET/MRI. Med Image Anal. 2015;19:110–20.

Grodzki DM, Jakob PM, Heismann B. Ultrashort echo time imaging using pointwise encoding time reduction with radial acquisition (PETRA). Magn Reson Med. 2012;67:510–8.

Gunzinger JM, Delso G, Boss A, Porto M, Davison H, von Schulthess GK, Huellner M, Stolzmann P, Veit-Haibach P, Burger IA. Metal artifact reduction in patients with dental implants using multispectral three-dimensional data acquisition for hybrid PET/MRI. EJNMMI Phys. 2014;1(1):102.

Hartung-Knemeyer V, Beiderwellen KJ, Buchbender C, Kuehl H, Lauenstein TC, Bockisch A, Poeppel TD. Optimizing positron emission tomography image acquisition protocols in integrated positron emission tomography/magnetic resonance imaging. Investig Radiol. 2013;48(5):290–4.

Johansson A, Karlsson M, Nyholm T. CT substitute derived from MRI sequences with ultrashort echo time. Med Phys. 2011;38:2708–14.

Jungmann PM, Agten CA, Pfirrmann CW, Sutter R. Advances in MRI around metal. J Magn Reson Imaging 2017. doi: https://doi.org/10.1002/jmri.25708. [Epub ahead of print] Review.

Kartmann R, Paulus DH, Braun H, Aklan B, Ziegler S, Navalpakkam BK, Lentschig M, Quick HH. Integrated PET/MR imaging: automatic attenuation correction of flexible RF coils. Med Phys. 2013;40:082301.

Keereman V, Fierens Y, Broux T, De Deene Y, Lonneux M, Vandenberghe S. MRI-based attenuation correction for PET/MRI using ultrashort echo time sequences. J Nucl Med. 2010;51:812–8.

Keereman V, Holen RV, Mollet P, Vandenberghe S. The effect of errors in segmented attenuation maps on PET quantification. Med Phys. 2011;38:6010–9.

Keller SH, Holm S, Hansen AE, Sattler B, Andersen F, Klausen TL, Højgaard L, Kjær A, Beyer T. Image artifacts from MR-based attenuation correction in clinical, whole-body PET/MRI. MAGMA. 2013;26(1):173–81.

Kinahan PE, Townsend DW, Beyer T, Sashin D. Attenuation correction for a combined 3D PET/CT scanner. Med Phys. 1998;25:2046–53.

Koesters T, Friedman KP, Fenchel M, Zhan Y, Hermosillo G, Babb J, Jelescu IO, Faul D, Boada FE, Shepherd TM. Dixon sequence with superimposed model-based bone compartment provides highly accurate PET/MR attenuation correction of the brain. J Nucl Med. 2016;57(6):918–24.

Ladefoged CN, Andersen FL, Keller SH, Löfgren J, Hansen AE, Holm S, Højgaard L, Beyer T. PET/MR imaging of the pelvis in the presence of endoprostheses: reducing image artifacts and increasing accuracy through inpainting. Eur J Nucl Med Mol Imaging. 2013;40(4):594–601.

Ladefoged CN, Hansen AE, Keller SH, Fischer BM, Rasmussen JH, Law I, Kjær A, Højgaard L, Lauze F, Beyer T, Andersen FL. Dental artifacts in the head and neck region: implications for Dixon-based attenuation correction in PET/MR. EJNMMI Phys. 2015;2(1):8. https://doi.org/10.1186/s40658-015-0112-5.

Ladefoged CN, Hansen AE, Keller SH, Holm S, Law I, Beyer T, Højgaard L, Kjær A, Andersen FL. Impact of incorrect tissue classification in Dixon-based MR-AC: fat-water tissue inversion. EJNMMI Phys. 2014;1(1):101. https://doi.org/10.1186/s40658-014-0101-0. Epub 2014 Dec 14

Lindemann ME, Oehmigen M, Blumhagen JO, Gratz M, Quick HH. MR-based truncation and attenuation correction in integrated PET/MR hybrid imaging using HUGE with continuous table motion. Med Phys. 2017;44(9):4559–72.

Manber R, Thielemans K, Hutton BF, Barnes A, Ourselin S, Arridge S, O'Meara C, Wan S, Atkinson D. Practical PET respiratory motion correction in clinical PET/MR. J Nucl Med. 2015;56:890–6.

Martinez-Moller A, Souvatzoglou M, Delso G, Bundschuh RA, Chefd'hotel C, Ziegler SI, Navab N, Schwaiger M, Nekolla SG. Tissue classification as a potential approach for attenuation correction in whole-body PET/MRI: evaluation with PET/CT data. J Nucl Med. 2009;50:520–6.

Navalpakkam BK, Braun H, Kuwert T, Quick HH. Magnetic resonance-based attenuation correction for PET/MR hybrid imaging using continuous valued attenuation maps. Investig Radiol. 2013;48:323–32.

Nuyts J, Bal G, Kehren F, Fenchel M, Michel C, Watson C. Completion of a truncated attenuation image from the attenuated PET emission data. IEEE Trans Med Imaging. 2013;32:237–46.

Nuyts J, Dupont P, Stroobants S, Benninck R, Mortelmans L, Suetens P. Simultaneous maximum a posteriori reconstruction of attenuation and activity distributions from emission sinograms. IEEE Trans Med Imaging. 1999;18:393–403.

Oehmigen M, Lindemann ME, Gratz M, Kirchner J, Ruhlmann V, Umutlu L, Blumhagen JO, Fenchel M, Quick HH. Impact of improved attenuation correction featuring a bone atlas and truncation correction on PET quantification in whole-body PET/MR. Eur J Nucl Med Mol Imaging. 2017 Nov 9. doi:10.1007/s00259-017-3864-4. [Epub ahead of print]

Oehmigen M, Lindemann ME, Lanz T, Kinner S, Quick HH. Integrated PET/MR breast cancer imaging: Attenuation correction and implementation of a 16-channel RF coil. Med Phys. 2016;43(8):4808.
Oehmigen M, Ziegler S, Jakoby BW, Georgi JC, Paulus DH, Quick HH. Radiotracer dose reduction in integrated PET/MR: implications from national electrical manufacturers association phantom studies. J Nucl Med. 2014;55(8):1361–7.
Paulus D, Braun H, Aklan B, Quick HH, Simultaneous PET. MR imaging: MR-based attenuation correction of local radiofrequency surface coils. Med Phys. 2012;39:4306–15.
Paulus DH, Oehmigen M, Grüneisen J, Umutlu L, Quick HH. Whole-body hybrid imaging concept for the integration of PET/MR into radiation therapy treatment planning. Phys Med Biol. 2016;61(9):3504–20.
Paulus DH, Quick HH. Hybrid positron emission tomography/magnetic resonance imaging: challenges, methods, and state of the art of hardware component attenuation correction. Investig Radiol. 2016;51:624–34.
Paulus DH, Quick HH, Geppert C, Fenchel M, Zhan Y, Hermosillo G, Faul D, Boada F, Friedman KP, Koesters T. Whole-body PET/MR imaging: quantitative evaluation of a novel model-based MR attenuation correction method including bone. J Nucl Med. 2015;56:1061–6.
Paulus DH, Tellmann L, Quick HH. Towards improved hardware component attenuation correction in PET/MR hybrid imaging. Phys Med Biol. 2013;58:8021–40.
Paulus DH, Thorwath D, Schmidt H, Quick HH. Towards integration of PET/MR hybrid imaging into radiation therapy treatment planning. Med Phys. 2014;41(7):072505.
Queiroz MA, Delso G, Wollenweber S, Deller T, Zeimpekis K, Huellner M, de Galiza Barbosa F, von Schulthess G, Veit-Haibach P. Dose Optimization in TOF-PET/MR Compared to TOF-PET/CT. PLoS One. 2015;10(7):e0128842.
Quick HH. Integrated PET/MR. J Magn Reson Imaging. 2014;39:243–58.
Quick HH, von Gall C, Zeilinger M, Wiesmüller M, Braun H, Ziegler S, Kuwert T, Uder M, Dörfler A, Kalender WA, Lell M. Integrated whole-body PET/MR hybrid imaging: clinical experience. Investig Radiol. 2013;48:280–9.
Rausch I, Quick HH, Cal-Gonzalez J, Sattler B, Boellaard R, Beyer T. Technical and instrumentational foundations of PET/MRI. Eur J Radiol. 2017;94:A3-A13. doi: 10.1016/j.ejrad.2017.04.004. Epub 2017 Apr 8. Review
Robson PM, Dweck MR, Trivieri MG, Abgral R, Karakatsanis NA, Contreras J, Gidwani U, Narula JP, Fuster V, Kovacic JC, Fayad ZA. Coronary Artery PET/MR imaging: feasibility, limitations, and solutions. JACC Cardiovasc Imaging. 2017. https://doi.org/10.1016/j.jcmg.2016.09.029. [Epub ahead of print]
Ruhlmann V, Heusch P, Kühl H, Beiderwellen K, Antoch G, Forsting M, Bockisch A, Buchbender C, Quick HH. Potential influence of Gadolinium contrast on image segmentation in MR-based attenuation correction with Dixon sequences in whole-body 18F-FDG PET/MR. MAGMA. 2016;29(2):301–8.
Samarin A, Burger C, Wollenweber SD, Crook DW, Burger IA, Schmid DT, von Schulthess GK, Kuhn FP. PET/MR imaging of bone lesions - implications for PET quantification from imperfect attenuation correction. Eur J Nucl Med Mol Imaging. 2012;39:1154–60.
Sander CY, Keil B, Chonde DB, Rosen BR, Catana C, Wald LL. A 31-channel MR brain array coil compatible with positron emission tomography. Magn Reson Med. 2015;73(6):2363–75.
Schramm G, Langner J, Hofheinz F, Petr J, Lougovski A, Beuthien-Baumann B, Platzek I, van den Hoff J. Influence and compensation of truncation artifacts in MR-based attenuation correction in PET/MR. IEEE Trans Med Imaging. 2013;32:2056–63.
Schramm G, Maus J, Hofheinz F, Petr J, Lougovski A, Beuthien-Baumann B, Platzek I, van den Hoff J. Evaluation and automatic correction of metal-implant-induced artifacts in MR-based attenuation correction in whole-body PET/MR imaging. Phys Med Biol. 2014;59(11):2713–26.
Schulz V, Torres-Espallardo I, Renisch S, Hu Z, Ojha N, Börnert P, Perkuhn M, Niendorf T, Schäfer WM, Brockmann H, Krohn T, Buhl A, Günther RW, Mottaghy FM, Krombach GA. Automatic, three-segment, MR-based attenuation correction for whole-body PET/MR data. Eur J Nucl Med Mol Imaging. 2011;38:138–52.
Seith F, Schmidt H, Kunz J, Kuestner T, Gatidis S, Nikolaou K, la Fougère C, Schwenzer NF. Simulation of tracer dose reduction in ^{18}F-FDG-Positron emission tomography / magnetic resonance imaging (PET/MRI): Effects on oncologic reading, image quality and artifacts. J Nucl Med. 2017. https://doi.org/10.2967/jnumed.116.184440. pii: jnumed.116.184440. [Epub ahead of print]
Sutter R, Ulbrich EJ, Jellus V, Nittka M, Pfirrmann CW. Reduction of metal artifacts in patients with total hip arthroplasty with slice-encoding metal artifact correction and view-angle tilting MR imaging. Radiology. 2012;265(1):204–14.
Talbot BS, Weinberg EP. MR Imaging with metal-suppression sequences for evaluation of total joint arthroplasty. Radiographics. 2016;36(1):209–25. https://doi.org/10.1148/rg.2016150075. Epub 2015 Nov 20. Review
Tellmann L, Quick HH, Bockisch A, Herzog H, Beyer T. The effect of MR surface coils on PET quantification in whole-body PET/MR: results from a pseudo-PET/MR phantom study. Med Phys. 2011;38(5):2795–805.
Ter Voert EE, Veit-Haibach P, Ahn S, Wiesinger F, Khalighi MM, Levin CS, Iagaru AH, Zaharchuk G, Huellner M, Delso G. Clinical evaluation of TOF versus non-TOF on PET artifacts in simultaneous PET/MR: a dual centre experience. Eur J Nucl Med Mol

Imaging. 2017. https://doi.org/10.1007/s00259-017-3619-2. [Epub ahead of print].

Tsoumpas C, Buerger C, King AP, Mollet P, Keereman V, Vandenberghe S, Schulz V, Schleyer P, Schaeffter T, Marsden PK. Fast generation of 4D PET-MR data from real dynamic MR acquisitions. Phys Med Biol. 2011;56:6597–613.

Tsoumpas C, Mackewn JE, Halsted P, King AP, Buerger C, Totman JJ, Schaeffter T, Marsden PK. Simultaneous PET-MR acquisition and MR-derived motion fields for correction of non-rigid motion in PET. Ann Nucl Med. 2010;24:745–50.

Wagenknecht G, Kaiser H-JJ, Mottaghy FM, Herzog H. MRI for attenuation correction in PET: Methods and challenges. Magn Reson Mater Phys Biol Med. 2013;26:99–113.

Wiesinger F, Sacolick LI, Menini A, Kaushik SS, Ahn S, Veit-Haibach P, Delso G, Shanbhag DD. Zero TE MR bone imaging in the head. Magn Reson Med. 2016;75:107–14.

Wiesmüller M, Quick HH, Navalpakkam B, Lell MM, Uder M, Ritt P, Schmidt D, Beck M, Kuwert T, von Gall CC. Comparison of lesion detection and quantitation of tracer uptake between PET from a simultaneously acquiring whole-body PET/MR hybrid scanner and PET from PET/CT. Eur J Nucl Med Mol Imaging. 2013;40(1):12–21.

Wollenweber SD, Delso G, Deller T, Goldhaber D, Hüllner M, Veit-Haibach P. Characterization of the impact to PET quantification and image quality of an anterior array surface coil for PET/MR imaging. MAGMA. 2014;27:149–59. Review

Wuerslin C, Schmidt H, Martirosian P, Brendle C, Boss A, Schwenzer NF, Stegger L. Respiratory motion correction in oncologic PET using T1-weighted MR imaging on a simultaneous whole-body PET/MR system. J Nucl Med. 2013;54:464–71.

Zaidi H, Ojha N, Morich M, Griesmer J, Hu Z, Maniawski P, Ratib O, Izquierdo-Garcia D, Fayad ZA, Shao L. Design and performance evaluation of a whole-body Ingenuity TF PET-MRI system. Phys Med Biol. 2011;56(10):3091–106.